Materials Chemistry and Physics 130 (2011) 1109–1117

Contents lists available at SciVerse ScienceDirect

Materials Chemistry and Physics

journal homepage: www.elsevier.com/locate/matchemphys

Formation mechanism of in situ Al_3Ti in Al matrix during hot pressing and subsequent friction stir processing

Q. Zhang, B.L. Xiao, D. Wang, Z.Y. Ma*

Shenyang National Laboratory for Materials Science, Institute of Metal Research, Chinese Academy of Sciences, Shenyang 110016, China

ARTICLE INFO

Article history:
Received 29 April 2011
Received in revised form 14 August 2011
Accepted 21 August 2011

Keywords:
Composite materials
Intermetallic compounds
Powder metallurgy
Friction stir processing

ABSTRACT

In situ Al_3Ti/Al composites were fabricated by a combination of vacuum hot pressing (VHP) and friction stir processing (FSP). The formation mechanism of the Al_3Ti and the effect of VHP and FSP parameters on the resultant microstructure and mechanical properties were investigated. The Al_3Ti formed due to the reactive diffusion between Al and Ti during VHP, and the number of Al_3Ti particles increased with increasing the temperature and holding time of the VHP. FSP not only induced the Al–Ti reaction, but also resulted in significant refining of the Al_3Ti, thereby creating a homogeneous distribution of Al_3Ti particles in the Al matrix. These microstructural changes led to significant improvement in the tensile properties of the in situ Al_3Ti/Al composite. However, the change trends of the tensile properties of the FSP samples were dependent on the extent of the Al–Ti reaction during VHP.

1. Introduction

In situ metal matrix composites (MMCs) are a type of multiphase material in which the reinforcements are synthesized in the metal matrix through chemical reactions during fabrication. Compared with ex situ MMCs, in situ MMCs have many advantages, such as a cleaner reinforcement–matrix interface, more thermodynamically stable reinforcements, better compatibility, and higher bonding strength between the reinforcements and the matrix [1]. In the last two decades, in situ aluminide particles (Al_3Ti, $NiAl_3$, $FeAl_3$, etc.) reinforced Al matrix composites (AMCs) attracted a great deal of attention due to their high specific strength, high specific modulus, and excellent mechanical properties at both ambient and elevated temperatures [2–5]. Among these composites, in situ Al_3Ti/Al composites are even more attractive because Al_3Ti has a relatively low density (3.4 g cm^{-3}) and high Young's modulus (220 GPa). Furthermore, the diffusivity and solubility of Ti in Al are low [5]. Hence, Al_3Ti is expected to exhibit a low coarsening rate at elevated temperature.

In previous studies, in situ Al_3Ti/Al composites were fabricated by powder metallurgy (e.g. sintering, hot pressing), and stirring casting [6–8]. However, the size of Al_3Ti in these composites was large (generally above 10 μm) because of high processing temperatures or coarse raw material powders. The coarse Al_3Ti blocks tend to crack under low stress during tensile tests, resulting in low strength and ductility. In situ Al_3Ti/Al composites fabricated by mechanical alloying (MA) exhibited high strength due to the presence of the fine Al_3Ti particles [5,9,10], but it is always accompanied by significant ductility loss due to inhomogeneous microstructures and contaminations introduced by MA. In addition, MA increases the cost and duration of production.

Friction stir processing (FSP), a development based on friction stir welding (FSW), is a new solid state processing technique for microstructural modification [11]. During FSP, the material in the processed zone undergoes intense plastic deformation, mixing, and thermal exposure, resulting in significant microstructural changes. The characteristics of FSP have led to several applications for microstructural modification in metallic materials, including enhanced superplasticity [12], surface composites [13], homogenization of nano-aluminum alloys and metal matrix composites [10], and microstructural refinement of cast alloys [14,15].

Not long ago, Kao and co-workers [16,17] fabricated in situ Al_3Ti/Al and $Al_{13}Fe_4$/Al composites using elemental powders via FSP. More recently, Ke et al. [18] fabricated in situ Al–Ni intermetallics reinforced aluminum matrix composites by FSP. These investigations [16–18] indicated that intense plastic deformation and a high temperature in FSP could induce the exothermic reaction between Al and other metals (Ti, Fe, Ni). However, it was also revealed that the exothermic reaction could not proceed to a sufficient level even after four-pass FSP with 100% overlapping. Furthermore, the reactive mechanism during FSP is still not very clear.

* Corresponding author. Tel.: +86 24 83978908; fax: +86 24 83978908.
E-mail address: zyma@imr.ac.cn (Z.Y. Ma).

0254-0584/$ – see front matter © 2011 Elsevier B.V. All rights reserved.
doi:10.1016/j.matchemphys.2011.08.042

Table 1
The parameters of VHP.

Sample	Temperature (°C)	Holding time (min)
Group 1	500	5
Group 2	600	120
Group 3	640	180

In this paper, we fabricated the Al_3Ti/Al composites using pure elemental powders through a combination of vacuum hot pressing (VHP) and FSP. Three groups of samples were fabricated by VHP, in which the reaction between Al and Ti was controlled to hardly, partially and completely occur, respectively. Then four-pass FSP with tool rotation rates of 1000 and 2000 rpm and a travel speed of 25 mm min^{-1} were adopted. The purpose of this study is (1) to understand the formation mechanism of the in situ Al_3Ti in the aluminum matrix during the VHP and FSP processes and (2) to elucidate the effect of the VHP and FSP parameters on the microstructure and tensile properties of the in situ Al_3Ti/Al composites.

2. Experimental procedure

The starting materials used in the present study were Al powder (99.9% purity, 13 μm) and Ti powder (99% purity, 45 μm). The nominal composition was Al–10%Ti (atom percent). The Al and Ti powders were mixed in a bi-axis rotary mixer for 12 h and then cold compacted into billets. The cold compacted billets were heated to the designated temperature in a vacuum furnace and then hot pressed after being held for a period of time. The temperature and holding time of the hot pressing for various billets are shown in Table 1. The hot pressed billets were 60 mm in diameter and 80 mm in height. In order to improve the ductility of the hot pressed billets and obtain sufficient size for the subsequent FSP, the hot pressed billets were forged in an open die under 200 MPa pressure at 480 °C. The total deformation ratio was 4:1. The forged plates were 120 mm in diameter and 20 mm in height.

Four-pass FSP with 100% overlapping was conducted on the forged billets at a travel speed of 25 mm min^{-1}. The tool rotation rates were 1000 and 2000 rpm, respectively. A steel tool with a concave shoulder 20 mm in diameter, a threaded conical pin 8 mm in root diameter, 5.5 mm in tip diameter, and 5.8 mm in length was used for FSP. The tool was made of H13 tool steel with a hardness of HRC 45.

The samples for microstructural investigations were cut transverse to the FSP direction. The microstructures were examined by scanning electron microscopy (SEM, Quanta 600) and transmission electron microscopy (TEM, TECNAI20). Thin foils for TEM were prepared by the ion-milling technique. Dogbone-shaped tensile specimens (5.0 mm gage length, 1.4 mm gage width, and 1.0 mm gage thickness) were electrical discharge machined from the stir zone (SZ) of the FSP samples transverse to the FSP direction. Tensile tests were conducted using an INSTRON 5848 micro-tester at an initial strain rate of 1×10^{-3} s^{-1}. The values for each condition were calculated by averaging the three test results. After tensile testing, the fracture surfaces were examined using SEM.

3. Results

3.1. Microstructure

Fig. 1(a) shows the XRD patterns of various samples in group 1. In the forged sample, the diffraction peaks of fcc-structured Al and hcp-structured Ti were detected. No Al_3Ti peaks were found, indicating that the reaction between Al and Ti did not take place during VHP and forging. By comparison, Al_3Ti peaks were found in the FSP samples, and XRD analysis indicated that the Al_3Ti had a tetragonal crystal system and body-centered lattice. The intensity of the Al_3Ti peaks increased as the tool rotation rate increased from 1000 to 2000 rpm. After four-pass FSP with a rotation rate of 2000 rpm, the Ti peaks still existed, indicating that the Ti did not react with the Al completely.

Table 2
Tensile properties of the forged and FSP samples at room temperature.

Materials		YS (MPa)	UTS (MPa)	Elongation (%)
Group 1	As forged	59	93	26
	FSP, 1000 rpm	220	250	15
	FSP, 2000 rpm	290	330	15
Group2	As forged	118	149	3
	FSP, 1000 rpm	315	368	10
	FSP, 2000 rpm	336	394	16
Group 3	As forged	171	208	3
	FSP, 1000 rpm	364	413	14
	FSP, 2000 rpm	323	377	15

Fig. 2 shows the microstructures of the various samples in group 1. In the forged sample, the coarse white particles were identified to be Ti. They were uniformly distributed in the Al matrix, and a few voids existed in the matrix. After four-pass FSP, the coarse Ti particles were refined and the voids were almost eliminated. As the tool rotation rate increased from 1000 to 2000 rpm, the size of the Ti particles decreased. The Al_3Ti was too fine to be revealed by SEM. Fig. 3(a) and (b) shows the TEM images of the FSP samples in group 1. It was revealed that the Al_3Ti particles formed in the Al matrix had an equiaxed shape and approximate sizes of 138 ± 45.7 nm and 142 ± 48.4 nm for the rotation rates of 1000 and 2000 rpm, respectively (averaging 140 particles).

The XRD patterns of the various samples in group 2 are shown in Fig. 1(b). For the forged sample, the Al_3Ti peaks were revealed and the Ti peaks were very weak, indicating that most of Ti reacted with Al to form Al_3Ti during VHP. For the FSP samples, only Al_3Ti and Al peaks were detected. Fig. 4 shows the microstructures of the various samples in group 2. In the forged sample, some core–shell structured particles with sizes of about 20–150 μm were observed (Fig. 4(a)). The light grey shell was identified to be Al_3Ti, and the white core was determined to be Ti. There were a few voids around the core–shell structured particles (Fig. 4(a) and (b)). Furthermore, some micro-cracks were found in the Al_3Ti shell (Fig. 4(b)).

Four-pass FSP resulted in the fundamental disappearance of the core–shell structured particles and the voids, and subsequently created a uniform distribution of fine Al_3Ti particles in the Al matrix. However, the core–shell structured particles were still visible in the FSP sample with a rotation rate of 1000 rpm (Fig. 4(c)). For the FSP sample with a rotation rate of 2000 rpm, the core–shell structured particles were broken up completely, whereas un-reacted Ti could still be occasionally detected (Fig. 4(d)), but the amount of Ti was too little to be detected by XRD. Image analyses based on the SEM images demonstrated that the average size of the Al_3Ti particles decreased from about 0.7 to 0.4 μm with increasing the tool rotation rate from 1000 to 2000 rpm (Fig. 4(c) and (d)). Some much smaller particles could not be resolved by the image analyzer. The TEM observations revealed the existence of numerous fine Al_3Ti particles with sizes of about 180–300 nm in the Al matrix of both FSP samples, the ones with rotation rates of 1000 and 2000 rpm (Fig. 3(c) and (d)).

Fig. 5 shows the microstructure of various samples in group 3. In the forged sample, the initial Ti reacted with Al completely to form Al_3Ti. The Al_3Ti particles had a size of about 0.5–3 μm, and the distribution was inhomogeneous (Fig. 5(a) and (b)). After four-pass FSP, the average size of the Al_3Ti decreased and the distribution of the Al_3Ti became homogeneous. However, the large Al_3Ti particles with sizes of 0.5–3 μm still existed, and increasing the tool rotation rate from 1000 to 2000 rpm caused no evident change in the distribution or size of the Al_3Ti particles (Fig. 5(c) and (d)). TEM observations indicated that a great number of the Al_3Ti particles with approximate sizes of 200 nm were uniformly distributed in the Al matrix of the FSP samples (Fig. 6). Increasing the tool rotation rate from 1000 to 2000 rpm caused little influence on the size and the distribution of the Al_3Ti particles, but the grain size of the matrix increased from about 0.5 to 1.0 μm (Fig. 6(a) and (b)).

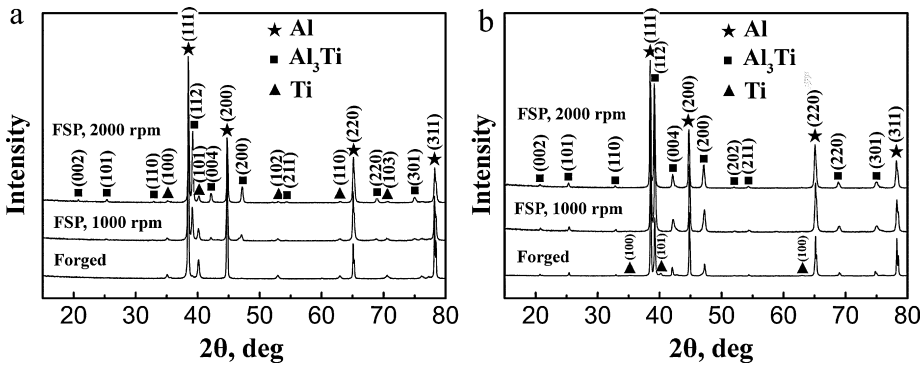

Fig. 1. XRD patterns of samples in (a) group 1 and (b) group 2.

3.2. Tensile properties and fractography

Table 2 summarizes the room temperature tensile properties of the forged and FSP samples. For group 1, the forged sample exhibited lower strengths and higher elongation. Four-pass FSP resulted in a significant improvement in yield strength (YS) and ultimate tensile strength (UTS), but a reduction in elongation. A higher tool rotation rate of 2000 rpm resulted in higher strength than that achieved at 1000 rpm. For group 2, the YS and UTS of the forged sample were higher than those of the forged sample in group 1 due to the Al_3Ti formation, but the elongation was reduced dramatically. After FSP, the YS, UTS and elongation were improved substantially and increased with increasing the rotation rate from 1000 to 2000 rpm. For group 3, the YS and UTS of the forged sample were higher than those of the forged samples in groups 1 and 2, but the elongation was almost identical compared to that of the forged sample in group 2. Four-pass FSP at a rotation rate of 1000 rpm increased the YS, UTS and elongation simultaneously. However, the YS and UTS decreased by 41 MPa and 36 MPa, respectively, with the increase of the rotation rate from 1000 to 2000 rpm, while the elongation increased slightly.

Fig. 7 shows the SEM fractographs of the FSP samples. For the FSP samples in group 1, the fracture surfaces were characterized by coarse dimples and some deep pits (Fig. 7(a)). With increasing the tool rotation rate from 1000 to 2000 rpm, the size of the dimples and the pits decreased substantially (Fig. 7(b)). The fracture surfaces of the FSP samples in group 2 showed shallow dimples (Fig. 7(c) and (d)). The sizes of the dimples were below 1 μm and decreased with increasing the tool rotation rate. On the fracture surface of the sample with a rotation rate of 1000 rpm, some deep pits could still be found (as shown by the white arrow in Fig. 7(c)). The fracture surfaces of the FSP samples in group 3 also exhibited ductile dimple fractures (Fig. 7(e) and (f)). Some dimples with sizes of about 1–3 μm were found except some fine dimples with the size

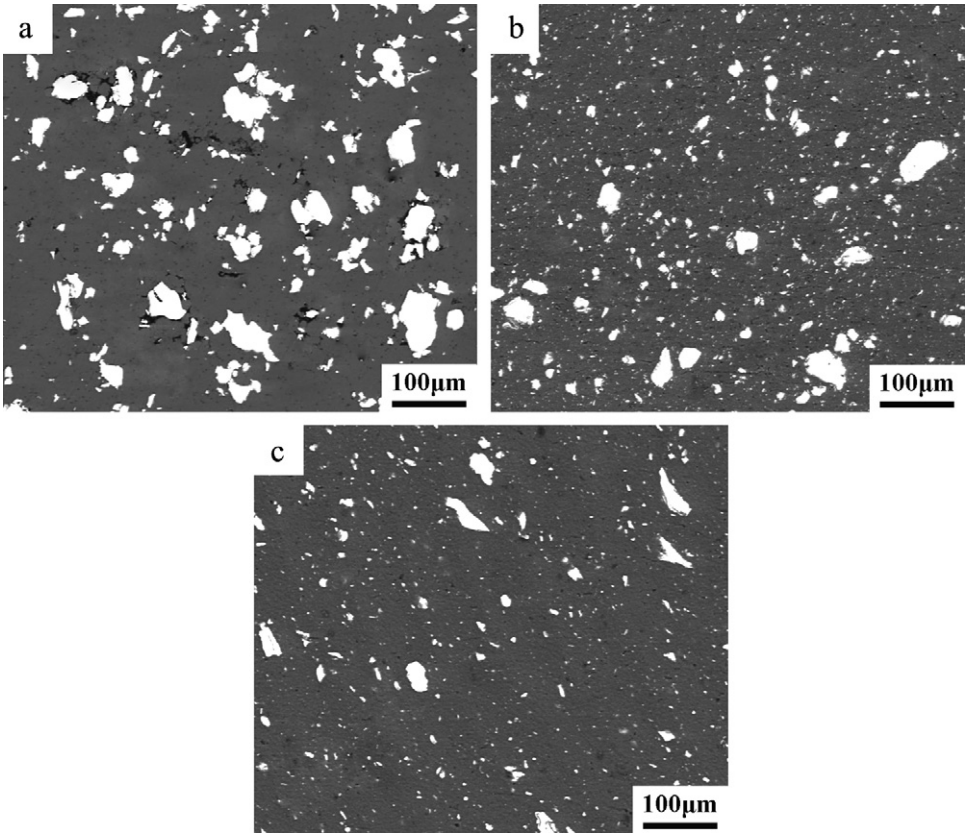

Fig. 2. SEM micrographs of samples in group 1: (a) forged; (b) FSP, 1000 rpm; and (c) FSP, 2000 rpm.

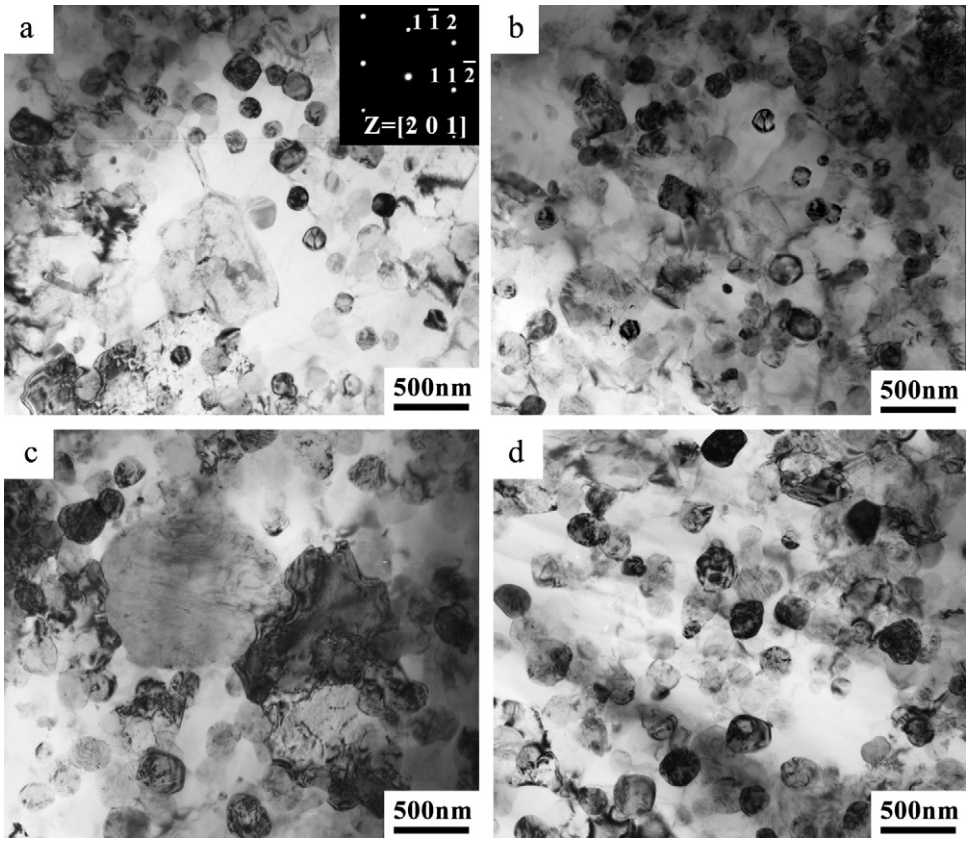

Fig. 3. TEM micrographs of FSP samples: (a) group 1, 1000 rpm; (b) group 1, 2000 rpm; (c) group 2, 1000 rpm; (d) group 2, 2000 rpm.

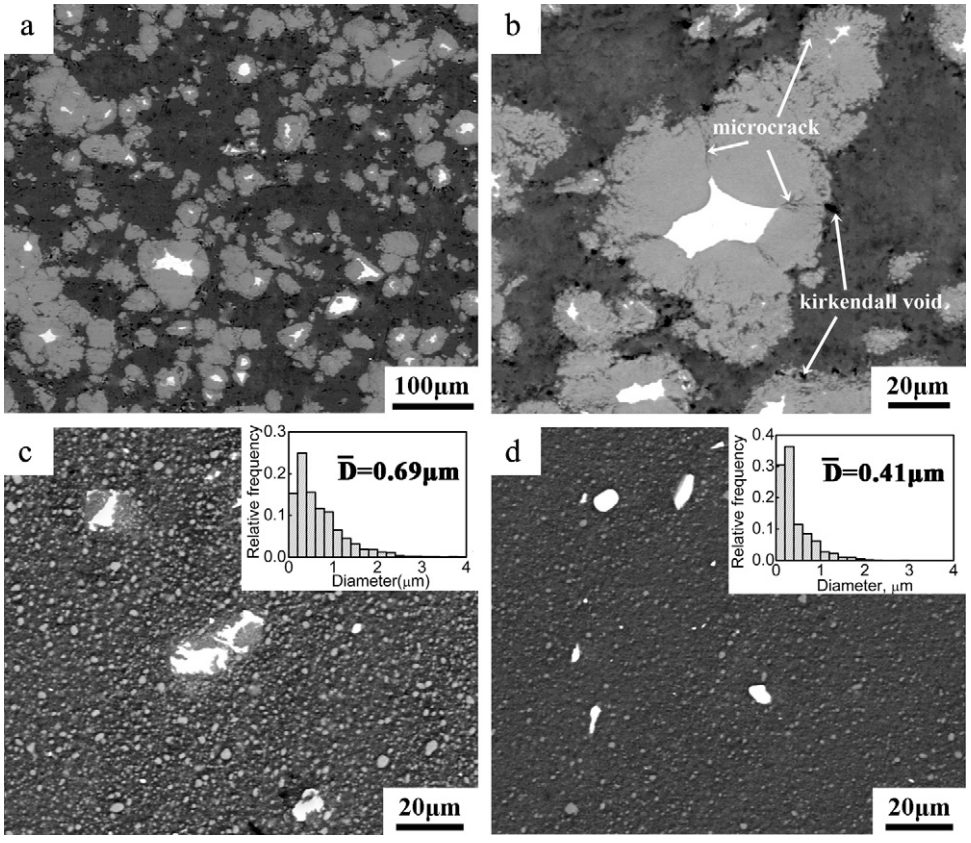

Fig. 4. SEM micrographs of samples in group 2: (a) and (b) forged; (c) FSP, 1000 rpm; and (d) FSP, 2000 rpm.

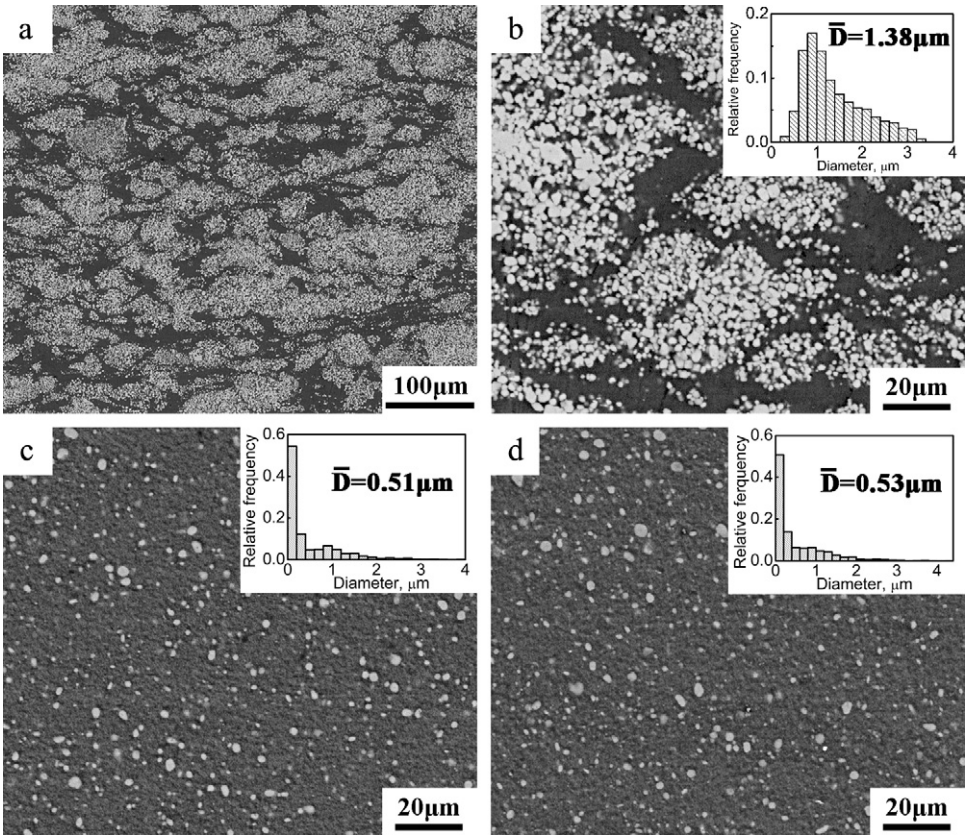

Fig. 5. SEM micrographs of samples in group 3: (a) and (b) forged; (c) FSP, 1000 rpm; and (d) FSP, 2000 rpm.

below 1 μm. Furthermore, increasing the tool rotation rate caused no evident change in the fracture surfaces of the FSP samples in group 3.

4. Discussion

4.1. Microstructure evolution during VHP

According to the Al–Ti binary phase diagram [19], in an Al–Ti solid diffusion couple, increasing the amount of Al in the Ti resulted in the formation of Ti_3Al, TiAl, Al_2Ti, and Al_3Ti layers, in this order. When the mass percentage of Ti is less than 37%, the final product of reactive diffusion in the Al–Ti system would be Al_3Ti after the system reached equilibrium state [19,20]. In this study, when the reactive diffusion between the Al and Ti powders occurred, some intermediate intermetallics might form. However, the diffusion coefficient of Al in Ti is much higher than that of Ti in Al ($D_{Al} \approx 1.5 \times 10^{-13}$ m^2 s^{-1} [21] and $D_{Ti} \approx 3.2 \times 10^{-17}$ m^2 s^{-1} at 600 °C [22]). Thus Al is always abundant during the diffusion. In this case, the intermediate intermetallics would transform to Al_3Ti [20]. Chianeh et al. [6] suggested that the transformation of various intermetallics from one form to another was faster than that of Ti to the intermetallics. Thus, in this study, only Al_3Ti existed in the forged samples.

The results of Chianeh et al. [6] showed that Al_3Ti formed after the green compact of Al–8.5 wt%Ti was sintered at 600 °C, and the growing rate of Al_3Ti layer was controlled by the diffusion of Ti in Al. Generally, in a reactive diffusion couple, the thickness of the reactive layer follows the parabolic law:

$$T^2 = Kt \tag{1}$$

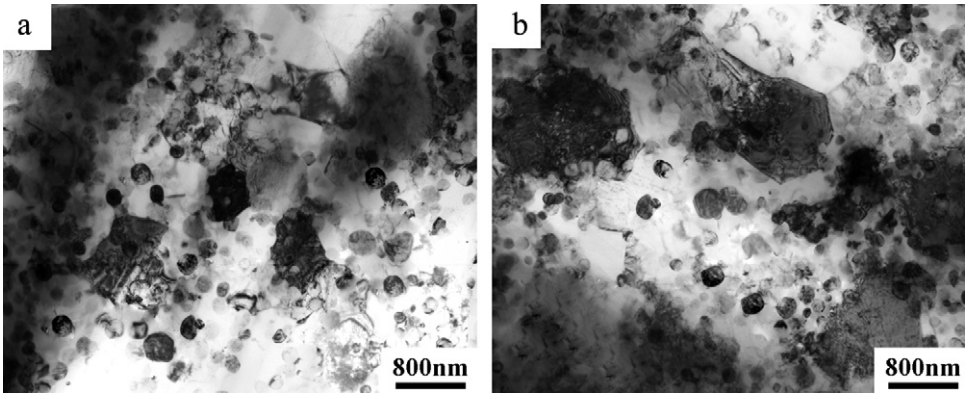

Fig. 6. TEM micrographs of FSP samples in group 3: (a) 1000 rpm, (b) 2000 rpm.

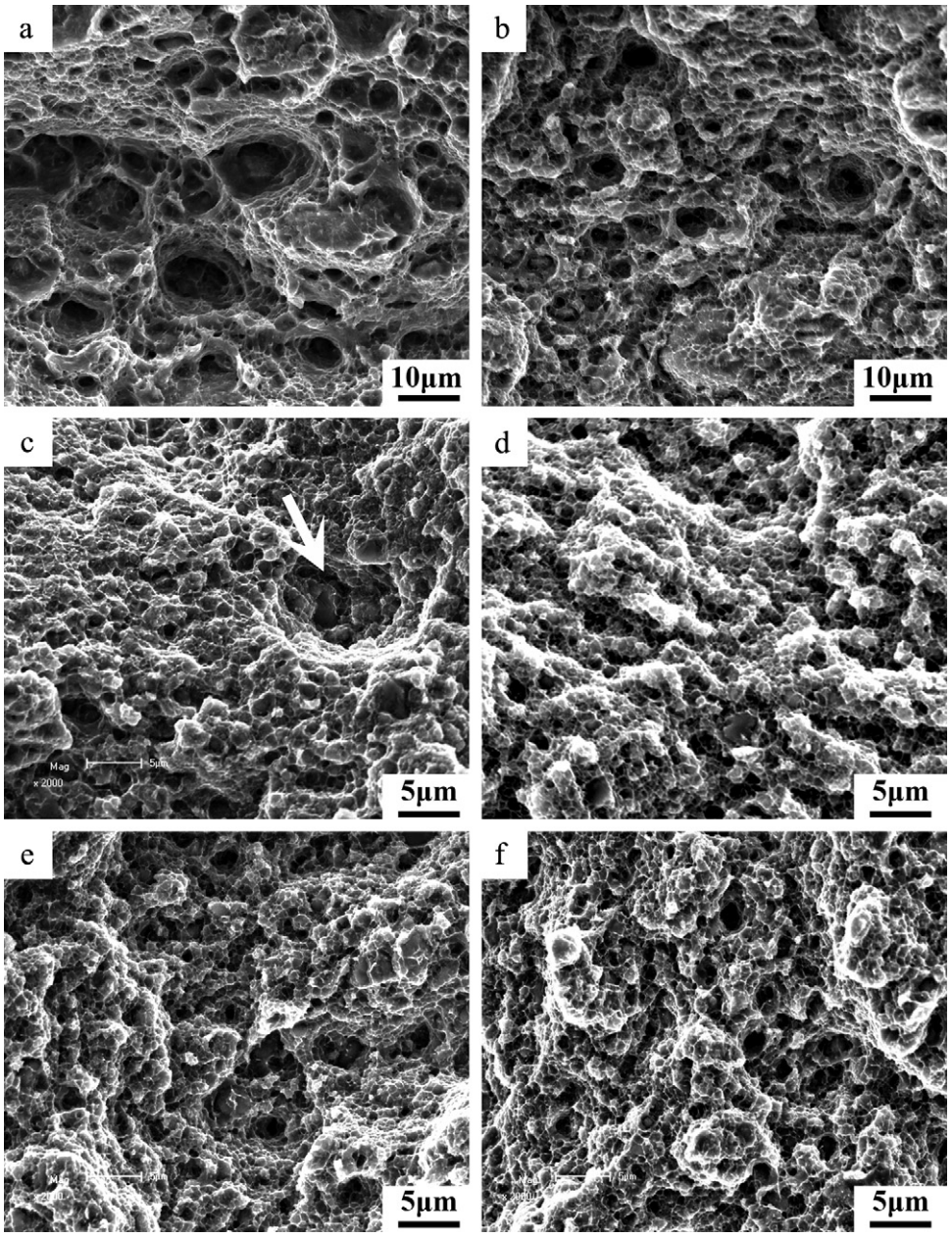

Fig. 7. Fracture surfaces of FSP samples: (a) group 1, 1000 rpm; (b) group 1, 2000 rpm; (c) group 2, 1000 rpm; (d) group 2, 2000 rpm; (e) group 3, 1000 rpm; (f) group 3, 2000 rpm.

where T is the thickness of the reactive layer, K is the constant related to the diffusion coefficient, and t is the diffusion time. The XRD and SEM results of the forged sample in group 1 revealed that the reaction between Al and Ti did not occur (Figs. 1(a) and 2(a)). This is attributed to the lower temperature and shorter holding time of VHP. With increasing the temperature and holding time of VHP, reactive diffusion took place between Al and Ti. The diffusion coefficient of Al in Ti is much higher than that of Ti in Al. Thus, the diffusion of Ti in Al can be neglected.

Fig. 8 gives the schematic diagrams illustrating the mechanism of the reactive diffusion between Al and Ti. At first, Al_3Ti formed at the outer layer of the initial Ti particles and formed the core–shell structure (Figs. 4(b) and 8(b)). The difference in the diffusion coefficients between Ti in Al during the Al–Ti inter-diffusion would produce vacancies in the Al as a result of Kirkendall's effect, thereby causing a volume expansion in Ti. Furthermore, the density of Al_3Ti is lower than that of Ti, so the formation of Al_3Ti would cause a considerable volume expansion. If the diffusion of Ti in Al was neglected, the percent of the volume expansion can be calculated by the following equation:

$$\frac{\Delta V}{V_{Ti}} = \frac{2.69\rho_{Ti}x}{\rho_{Al_3Ti}} - x \quad (2)$$

where $\Delta V/V_{Ti}$ is the percentage of the volume expansion of Ti, x is the weight percentage of reacted Ti, $\rho_{Ti} = 4.5\,g\,cm^{-3}$ and $\rho_{Al_3Ti} = 3.4\,g/cm^3$. The volume expansion percentage would be 256% if a Ti particle was transformed into Al_3Ti completely according to Eq. (2). Chinaeh et al. [6] suggested that the volume expansion would produce tensile stresses in the outer layer of the particles and compressive stress in the core of the particles, and this resulted in the initiation of some miro-cracks in Al_3Ti as the reaction proceeded. The number of micro-cracks increased with the volume expansion (Fig. 4(b)). The large brittle Al_3Ti blocks were easily broken into

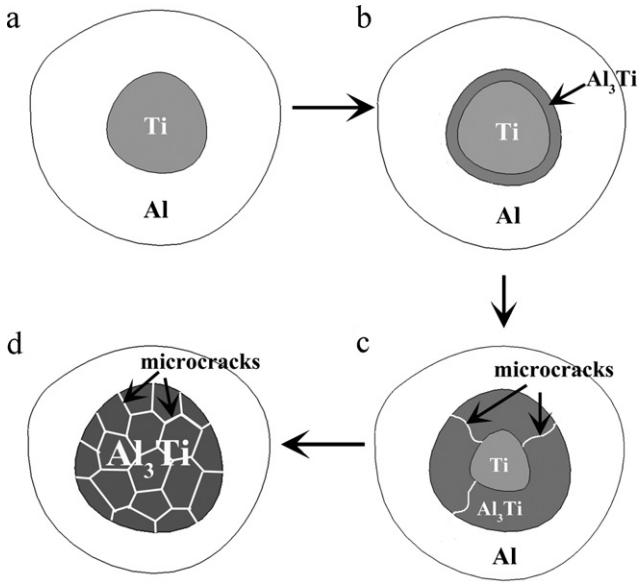

Fig. 8. Schematic diagrams of reactive mechanism between Al and Ti.

smaller blocks with sizes of 0.5–3 μm during forging due to the existence of these miro-cracks (Fig. 5(a) and (b)).

Furthermore, Fig. 2(a) indicates that after VHP with lower temperature and shorter holding time, there were a few voids in the Al matrix. This phenomenon was observed in many billets fabricated by PM at lower temperatures. Tang et al. [23] pointed out that there was some chemisorbed water incorporated into the oxide film of the aluminum particle, and Quadrapole Mass Spectrometry (QMS) measurements verified that the chemisorbed water could not be removed by vacuum heating until the temperature reached about 550 °C. Therefore, at temperatures below 550 °C, the sintering neck could not be developed and the densification of the compact of Al was difficult [23]. Increasing the temperature and holding time of VHP caused these voids to disappear due to the removal of the chemisorbed water and the enhanced diffusion between the Al particles in contact. However, a few voids were detected around the boundaries of Al_3Ti at higher pressing temperatures (Fig. 4(a) and (b)). The formation of these voids was attributed to the Kirkendall's effect as discussed above. Kirkendall's effect caused more vacancies in the Al, and the vacancies would coalesce into the voids when they reached supersaturated state in the Al [6] (Fig. 4(b)). When the diffusion from Al to Ti finished, the Kirkendall voids would disappear due to the lengthy diffusion at relatively high temperature during VHP.

4.2. Microstructure evolution during FSP

For the samples in group 1, XRD results revealed the formation of the Al_3Ti in the FSP samples, and the number of Al_3Ti increased as the tool rotation rate increased from 1000 to 2000 rpm (Fig. 1(a)). This fact indicated that the reaction between Al and Ti occurred during FSP. The peak temperatures of the SZ, recorded by embedding thermocouples in the regions adjacent to the rotating pin, were generally reported to be in the range of 400–500 °C in FSW/FSP aluminum alloys [14,24,25], which is below the reactive temperature between Al and Ti recorded by DSC [16] and even the VHP temperature for group 1. However, it is important to point out that the maximum temperature during FSP/FSW should be higher than the peak temperature recorded by the thermocouples because the thermocouples were actually located outside the region stirred by the rotating pin. In the present case, the heat release due to the in situ chemical reaction during FSP could also contribute to the temperature rise. Thus, it is very likely that the peak temperature of the SZ in the present study might be higher than that reported for FSP/FSW aluminum alloys.

During FSP, the material in the SZ underwent intense plastic deformation and thermal exposure. It was estimated that one-pass FSP could produce an effective strain of >40 [26]. First, the large plastic deformation of FSP broke up the oxide film surrounding Al, which caused intimate contact between Al and Ti. Second, intense plastic deformation reduced the diffusion distance and enhanced the diffusion rate [27]. Third, Biallas et al. [28] suggested that the materials flow around the pin was somewhat similar to that mechanical milling of metal. Mechanical milling could reduce the activation energy and the reactive temperature of the Al–Ti, Al–Ti–B and Al–TiO_2 systems [20,29]. Thus, the reactive temperature between Al and Ti during FSP was believed to be lower than that obtained from the DSC curve.

Based on the above factors, one can consider that the heat provided by FSP could raise the temperature to a level high enough to induce the reaction between Al and Ti. Once the Al_3Ti formed at the Al–Ti interface, the large plastic strain imposed in FSP could effectively remove it immediately. In this case, direct contact between Al and Ti could be maintained, and the reaction could proceed rapidly at the interface. Since the Al_3Ti was removed rapidly from the interface and the duration of the thermal exposure in FSP was very short, the growth of the particles was limited, and nanometer-sized particles were obtained. Increasing the rotation rate from 1000 to 2000 rpm caused a higher peak temperature in the SZ [25]. Thus the reaction between Al and Ti became easier, resulting in the increase of the volume fraction of Al_3Ti. Because the coarsening rate of the Al_3Ti particles is very low at about 600 °C ($\sim 5.2 \times 10^{-24}$ m^3 s^{-1} at 630 °C [22]), the size of Al_3Ti hardly changed in the FSP samples as the tool rotation rate increased. Thus, increasing the tool rotation rate from 1000 to 2000 rpm resulted in the increase of the number of the Al_3Ti particles. Because the Ti powders in this study was coarse (45 μm) and the duration of FSP was very short, there were still some un-reacted Ti after four-pass FSP with a rotation rate of 2000 rpm. This result is consistent with the reference [16]. This fact also indicated that in order to achieve a complete reaction between Ti and Al during FSP, fine Ti particles should be adopted.

For the samples in group 2, a great amount of Al_3Ti formed around the Ti particles, and the core–shell structure was generated during VHP (Fig. 4(a)). FSP broke up the core–shell structure and promoted the reaction between the residual Ti and Al simultaneously. Fig. 4(c) and (d) shows that the size of Al_3Ti in the FSP samples decreased substantially compared with that in the forged sample and decreased as the tool rotation rate increased from 1000 to 2000 rpm. The material flow during FSP is a complicated process. It is proposed that the threaded pin results in a superimposed vertical and horizontal material flow from geometrical considerations [30,31]. The threads tend to move material downward along the pin wall, and once this material reaches the bottom, the geometrical constraints require that the material move up and away from the pin wall. The lateral traverse of the pin requires that the material move from front to back. The interaction along these three material flow patterns caused a thorough mixing of material and substantial refinement of coarse second phase particles in the SZ. Increasing the tool rotation rate resulted in more intense material deformation and more thorough mixing, which broke up the core–shell structure completely and decreased the size of Al_3Ti particles.

However, the Al_3Ti particles revealed by TEM in the FSP samples of group 2 were coarser than those in the FSP samples of group 1. This can be attributed to the different forming mechanisms of Al_3Ti in the two groups. As discussed above, the Al_3Ti particles in the FSP samples of group 1 were in situ formed during FSP. While the severe plastic deformation and elevated temperature during FSP promoted the nucleation of Al_3Ti, the short duration of the

thermal exposure in FSP limited the coarsening of Al_3Ti. Therefore, the finer Al_3Ti particles were obtained in the FSP samples of group 1. Meanwhile, for the samples of group 2, the Al_3Ti blocks were mostly formed during VHP, and then significantly refined by multiple-pass FSP. Previous studies suggested that when the size of the particles was reduced to a certain value, the particles might flow with the flow deformation of the matrix during FSP [14,32,33]. In this case, the refinement of the second phase particles by FSP was limited. For example, Azizieh et al. [32] fabricated nano Al_2O_3 particles reinforced AZ31 composites via FSP. After four-pass FSP with different rotation rates, the average size of the Al_2O_3 clusters could not be reduced below 230 nm. Similarly, Zahmatkesh et al. [33] reported the smallest particle clusters of about 200 nm in the nano Al_2O_3 particles reinforced 2024 surface composites fabricated by FSP.

For the samples in group 3, the initial Ti reacted with Al to form Al_3Ti completely in the forged sample (Fig. 5(a) and (b)). FSP broke up and redistributed the Al_3Ti particles (Fig. 5(c) and (d)). However, because the Al_3Ti particles were reduced to 0.5–3 μm in size in the forged sample and exhibited the cobble shape, the refinement of the Al_3Ti was not significant compared with that in the samples of group 2. Increasing the rotation rate from 1000 to 2000 rpm caused almost no further refinement of Al_3Ti due to the enhanced material flowability under the higher heat input. In addition, the size of the fine Al_3Ti particles revealed by TEM was still about 200 nm, which is similar to that in the FSP samples of group 2.

4.3. Tensile properties

As presented in Fig. 2(a), the microstructure of the forged sample in group 1 consisted of coarse Ti particles and Al matrix. The large Ti particles did not exert a significant strengthening effect on the Al matrix, so the forged sample in group 1 exhibited lower strength and higher elongation. FSP resulted in a significant improvement in strength and a reduction in ductility for the samples in group 1. This is attributed to the following two factors. First, the ultra-fine Al_3Ti particles formed during FSP, as shown in Fig. 3, exerted a remarkable strengthening effect on the Al matrix through the Orawan bowing mechanism. Second, although there were still some Ti particles in the Al matrix after FSP, their size was substantially reduced (Fig. 2(b) and (c)). The finer Ti particles would exert an additional strengthening effect on the Al matrix due to possessing higher strength than Al. The large deep pits on the fracture surface of the FSP sample prepared at 1000 rpm were associated with the pullout of the Ti particles (Fig. 7(a)). Increasing the tool rotation rate from 1000 to 2000 rpm resulted in the generation of more Al_3Ti particles (Figs. 1(a) and 3) and the refinement of the Ti particles (Fig. 2(b) and (c)), thus the strength was improved with increasing the tool rotation rate. Accordingly, the size of the deep pits on the fracture surface of the FSP sample prepared at 2000 rpm was significantly reduced (Fig. 7(b)).

For the forged sample in group 2, the Al_3Ti blocks formed during VHP (Fig. 4(a) and (b)), resulting in higher strength than that of the forged sample in group 1. However there were some micro-cracks in the coarse Al_3Ti blocks (Fig. 4(b)). The Al_3Ti blocks tended to crack early during tensile deformation, resulting in a remarkable reduction in ductility. By comparison, the strength and ductility of the FSP samples was substantially enhanced and increased with increasing the rotation rate from 1000 to 2000 rpm. This is attributed to two factors. First, substantial refining of coarse Al_3Ti particles by four-pass FSP, as shown in Fig. 4, significantly reduced the possibility of the Al_3Ti particle cracking under low stress and consequently minimized the possibility of void initiation, thereby increasing the strength and ductility simultaneously. Second, FSP induced the Al–Ti reaction to form nano-sized Al_3Ti particles, which exerted an additional strengthening effect on the Al matrix. In the FSP sample with a rotation rate of 1000 rpm, some Al_3Ti blocks with the core–shell structure could be observed (Fig. 4(c)). These blocks would crack preferentially during tension and leave the pits on the fracture surface (white arrow in Fig. 7(c)). So the FSP sample with a rotation rate of 1000 rpm exhibited a relatively lower elongation (10%). Increasing the tool rotation rate led to a sufficient breakup of the Al_3Ti blocks and decreased the size of Al_3Ti particles (Fig. 4(c) and (d)), thus the strength and ductility of the FSP samples increased with increasing the tool rotation rate from 1000 to 2000 rpm.

The strength of the forged sample in group 3 was higher than that in groups 1 and 2. This is attributed to the fact that all the Ti particles reacted with Al to form Al_3Ti (Fig. 5), and the size of the Al_3Ti was finer than that in the forged sample in group 2 (Figs. 4 and 5). However, the distribution of the Al_3Ti is inhomogeneous (Fig. 5(a) and (b)), so the forged sample still exhibited low ductility. FSP resulted in a significant improvement in both strength and ductility. This is attributed to the refinement and redistribution of the Al_3Ti by FSP. The strength of the FSP samples decreased with increasing the rotation rate from 1000 to 2000 rpm. This is different from the results for the samples in groups 1 and 2. As shown in Figs. 5 and 6, the size and distribution of Al_3Ti did not change evidently when the rotation rate increased from 1000 to 2000 rpm, and further, the fracture surfaces of the samples with different rotation rates were also similar (Fig. 7(e) and (f)). Thus the decrease of the strength would be attributed to the increase in the grain size of the matrix.

The influence of the grain size on the matrix strength can be described by the Hall–Petch relationship:

$$\sigma = \sigma_0 + \frac{k}{\sqrt{d}} \tag{3}$$

where d is the grain size, σ_0 is 13 MPa and k = 74 MPa μm$^{1/2}$ for pure Al [34]. In the present study, TEM observations indicated that the grain size of the matrix increased from about 0.5 to 1.0 μm when the tool rotation rate increased from 1000 to 2000 rpm. According to Eq. (3), the decrease of the matrix strength would be 32 MPa. For particle reinforced MMCs, the influence of the matrix strength on the composite strength can be described by the modified shear lag model [35]:

$$\sigma_c = \sigma_m \left[\frac{V_p(s+2)}{2} + 1 - V_p \right] \tag{4}$$

where σ_c and σ_m are the strengths of the composite and the matrix, respectively, V_p and s are the volume fraction and aspect ratio of the reinforcements, respectively. For the FSP samples in group 3, Ti particles completely reacted with the Al matrix to form Al_3Ti. Therefore, the volume fraction of Al_3Ti was calculated to be 38.7%. The value of s was determined to be 1 because the Al_3Ti particles were nearly equiaxed in the present study. According to Eq. (4), the decrease in the strength of the composites would be 38.2 MPa when the tool rotation rate increased from 1000 to 2000 rpm, which is comparable with the experimental data (41 MPa).

Comparing all the investigated samples fabricated by three different procedures with two different tool rotation rates, the FSP sample with a rotation rate of 1000 rpm in group 3 exhibited the optimal combination of strength and ductility. This is attributed to the existence of a great number of fine and uniformly distributed Al_3Ti particles and the complete elimination of un-reacted Ti particles.

5. Conclusions

(1) In situ Al_3Ti/Al composites were fabricated by a combination of VHP and FSP. For VHP at a temperature of 500 °C with a holding

time of 5 min, the Al–Ti reaction hardly took place. For VHP at a temperature of 600 °C with a holding time of 120 min, the Al–Ti reaction took place mostly to form the core–shell structured particles due to reactive diffusion. For VHP at a temperature of 640 °C with a holding time of 180 min, all the Ti particles reacted with Al to form Al_3Ti 0.5–3 μm in size.

(2) For the VHP samples without the Al–Ti reaction, subsequent FSP induced the Al–Ti reaction to form nano-sized Al_3Ti particles in the Al matrix. Increasing the tool rotation rate from 1000 to 2000 rpm resulted in the formation of more Al_3Ti particles, thus the strength was improved with increasing the tool rotation rate. However, un-reacted Ti particles still existed after four-pass FSP even at the tool rotation rate of 2000 rpm.

(3) For the VHP samples with the Al–Ti reaction occurring mostly, subsequent FSP broke up the core–shell structured particles, promoted the Al–Ti reaction, and created a homogeneous distribution of Al_3Ti particles in the Al matrix. The size of the Al_3Ti particles decreased as the tool rotation rate increased from 1000 to 2000 rpm. Thus, the strength of the FSP samples increased with increasing the tool rotation rate from 1000 to 2000 rpm.

(4) For the VHP samples with Al–Ti reactions going to completion, subsequent FSP resulted in a uniform distribution of the Al_3Ti in the Al matrix. However, the refining of the Al_3Ti during FSP was not significant. The strength of the FSP samples decreased as the rotation rate increased from 1000 to 2000 rpm because of the increased grain size.

(5) Among the FSP samples fabricated under different conditions, the sample with the completed Al–Ti reaction during VHP and then processed at a tool rotation rate of 1000 rpm exhibited an optimal combination of strength and ductility. The YS, UTS and elongation were 364 MPa, 413 MPa and 14%, respectively.

Acknowledgements

This work was supported by the National Natural Science Foundation of China under grant no. 50890171, the National Basic Research Program of China under grant no. 2011CB606301, and the National Outstanding Young Scientist Foundation under grant no. 50525103.

References

[1] S.C. Tjong, Z.Y. Ma, Mater. Sci. Eng., R 29 (2000) 49.
[2] D. Roy, S. Ghosh, A. Basumallick, B. Basu, J. Alloys Compd. 436 (2007) 107.
[3] Z.Y. Ma, S.C. Tjong, Metall. Mater. Trans. A 28 (1997) 1931.
[4] S. Srinivasan, S.R. Chen, R.B. Schwarz, Mater. Sci. Eng. A 153 (1992) 691–695.
[5] S.H. Wang, P.W. Kao, Acta Mater. 46 (1998) 2675.
[6] V.A. Chianeh, H.R.M. Hosseini, M. Nofar, J. Alloys Compd. 473 (2009) 127.
[7] K. Das, L.K. Narnaware, Mater. Charact. 60 (2009) 808.
[8] R.A. Varin, Metall. Mater. Trans. A 33 (2002) 193.
[9] R.W. Hayes, R. Rodriguez, E.J. Lavernia, Acta Mater. 49 (2001) 4055.
[10] S.S. Nayak, S.K. Pabi, B.S. Murty, J. Alloys Compd. 492 (2010) 128.
[11] R.S. Mishra, M.W. Mahoney, S.X. Mcfadden, N.A. Mara, A.K. Mukherjee, Scripta Mater. 42 (2000) 163.
[12] Z.Y. Ma, R.S. Mishra, M.W. Mahoney, R. Grimes, Mater. Sci. Eng. A 351 (2003) 148.
[13] R.S. Mishra, Z.Y. Ma, I. Charit, Mater. Sci. Eng. A 341 (2003) 307.
[14] Z.Y. Ma, S.R. Sharma, R.S. Mishra, Metall. Mater. Trans. A 37 (2006) 3323.
[15] A.H. Feng, Z.Y. Ma, Scripta Mater. 56 (2007) 397.
[16] C.J. Hsu, C.Y. Chang, P.K. Kao, N.J. Ho, C.P. Chang, Acta Mater. 54 (2006) 5241.
[17] I.S. Lee, P.W. Kao, N.J. Ho, Intermetallics 16 (2008) 1104.
[18] L.M. Ke, C.P. Huang, X. Li, K.H. Huang, J. Alloys Compd. 503 (2010) 494.
[19] L.F. Mondolfo, Aluminum Alloys: Structure and Properties, Butterworth & Co. Ltd, London, 1976.
[20] L. Lü, M.O. Lai, Mechanical Alloying, Kluwer Academic Publishers, London, 1998.
[21] Y. Mishin, C.H.R. Herzig, Acta Mater. 48 (2000) 589.
[22] I.C. Barlow, H. Jones, W.M. Rainforth, Acta Mater. 49 (2001) 1209.
[23] F. Tang, I.E. Anderson, S.B. Biner, J. Light Met. 2 (2002) 201.
[24] M.W. Mahoney, C.G. Rhodes, J.G. Flintoff, R.A. Spurling, W.H. Bingel, Metall. Mater. Trans. A 29 (1998) 1955.
[25] W. Tang, X. Gao, J.C. Mcclure, L.E. Murr, J. Mater. Process. Manuf. Sci. 7 (1998) 163.
[26] P. Heurtier, C. Desrayaud, F. Montheillet, Mater. Sci. Forum 396–402 (2002) 1537.
[27] Z.Y. Ma, A.L. Pilchak, M.C. Juhas, J.C. Williams, Scripta Mater. 58 (2008) 361.
[28] G. Biallas, R. Braun, C.D. Donne, G. Staniek, W.A. Keysser, Proc. 1st Int. Symp. Friction Stir. Welds, Thousand Oaks, CA, 1999.
[29] N.J. Welham, Mater. Sci. Eng. A 255 (1998) 81.
[30] T.U. Seidel, A.P. Reynolds, Metall. Mater. Trans. A 32 (2001) 2879.
[31] A.P. Reynolds, Sci. Technol. Weld. Joining 5 (2000) 120.
[32] M. Azizieh, A.H. Kokabi, P. Abachi, Mater. Des. 32 (2011) 2034.
[33] B. Zahmatkesh, M.H. Enayati, Mater. Sci. Eng. A 527 (2010) 6734.
[34] C.Y. Yu, P.W. Kao, P.C. Chang, Acta Mater. 53 (2005) 4019.
[35] V.C. Nardone, K.M. Prewo, Scripta Mater. 20 (1986) 43.